applied optics

Ambient temperature-independent dual-band mid-infrared radiation thermometry

You Lü,[1,2] Xin He,[1,*] Zhong-Hui Wei,[1] Zhi-Yuan Sun,[1] and Song-Tao Chang[1]

[1]Changchun Institute of Optics, Fine Mechanics and Physics, Chinese Academy of Sciences, Changchun, Jilin 130033, China
[2]University of Chinese Academy of Science, Beijing 100049, China
*Corresponding author: hexin6627@sohu.com

Received 26 November 2015; revised 23 January 2016; accepted 24 January 2016; posted 25 January 2016 (Doc. ID 254603); published 15 March 2016

For temperature measurements of targets at low temperatures, dual-band radiation thermometry using mid-infrared detectors has been investigated extensively. However, the accuracy is greatly affected by the reflected ambient radiation and stray radiation, which depend on the ambient temperature. To ensure measurement accuracy, an improved dual-band measurement model is established by considering the reflected ambient radiation and the stray radiation. The effect of ambient temperature fluctuation on temperature measurement is then further analyzed in detail. Experimental results of measuring a gray-body confirm that the proposed method yields high accuracy at varying ambient temperatures. This method provides a practical approach to remove the effect of ambient temperature fluctuations on temperature measurements.

OCIS codes: (120.6780) Temperature; (120.5630) Radiometry; (120.4640) Optical instruments; (110.3080) Infrared imaging; (110.6820) Thermal imaging.

http://dx.doi.org/10.1364/AO.55.002169

1. INTRODUCTION

Temperature is one of the most important characteristics of scientific, industrial, and military targets. Temperature measurement thus acts as a key role in target detection, monitoring, and diagnosis processes [1–3]. Numerous methods for temperature measurement have been developed in the past years, such as thermocouples and radiation thermometers [4].

Radiation-based thermometry is intensively exploited due to its noncontact nature and harmlessness to a target [5]. In dual-band radiation thermometry, as one of the most important approaches in radiation thermometry, the target signal is collected by a dual-band thermometer in two different spectral bands simultaneously. The absolute temperature is determined using the ratio form when regarding the target as a gray-body with an unknown emissivity [6]. However, the total radiation collected in each band contains not only the radiation emitted from the target but also the ambient radiation reflected by the target and the stray radiation inside the measurement system [7]. The reflected ambient radiation and stray radiation, which are related to the ambient temperature, would greatly affect the measurement accuracy of the dual-band mid-infrared radiation thermometry (DMRT), especially for low-temperature measurements [8]. Various methods have been proposed to eliminate these drawbacks. Most researchers remove the influence of reflected ambient radiation by subtracting it from the total collected radiation in a mathematical method [9,10]; others control the reflected radiation using special structures [11,12]. For instance, Araújo *et al.* placed a low-temperature pyrometer inside an enclosure with controlled inner surface temperature. As for the stray radiation, it is regarded as the radiation from the internal components, such as the optical system and other mechanical structures; however, the specific way to deal with it has not been detailed in the literature.

In addition, for a dual-band radiation thermometer based on a mid-wave infrared (MWIR) detector, the radiometric calibration must be performed prior to the temperature measurement [13]. Moreover, the ambient temperature during the measurement process, in practice, is always different from that of calibration [7]. For example, radiometric calibration may be performed in the laboratory rather than in the field, and the temperature measurement process may last for a long time, and both of these may result in a change of the reflected ambient radiation and stray radiation, thus restricting the accuracy [8]. Because the aforementioned radiations vary with the ambient temperature, frequent calibration must be conducted before the temperature measurement to retain measurement accuracy. However, the calibration process is complicated and time consuming. As a consequence, a comprehensive analysis simultaneously taking both the reflected ambient radiation and the stray radiation into account is required to study the effect of ambient temperature on DMRT.

In this paper, we propose an improved dual-band thermometry by considering both the contribution of reflected radiation and stray radiation, and we also analyze the effect of ambient temperature on temperature measurement. Experimental results of a gray-body ranging from 50°C to 120°C illustrate that our method yields high measurement accuracy even under fluctuating ambient temperatures. This method provides an approach to estimate the absolute target temperature without repeated calibration when the ambient temperature fluctuates.

2. DMRT BASED ON A COOLED MWIR DETECTOR

As an extension of single-band radiation thermometry, dual-band radiation thermometry can eliminate the effect of unknown emissivity on temperature measurements. It measures the radiation in two different spectral bands, and the absolute temperature of a target can be determined by their ratios (assuming the emissivity is constant at the two close wavebands) [14]. Radiometric calibrations in each band must be individually performed prior to the calibration of the dual-band thermometer [13]. In this section, we first introduce improved dual-band thermometry by considering reflected ambient radiation and stray radiation, and the effect of ambient temperature fluctuation on dual-band thermometry is further discussed. Finally, a ratio formula applied to fluctuating ambient temperature is proposed.

A. DMRT Considering Reflected Ambient Radiation and Stray Radiation

1. Radiometric Calibration

To achieve the response and offset of a dual-band radiation thermometer, the radiometric calibration of each band should be conducted first. In the linear response range of a cooled MWIR detector, the relation between the output gray value [digital number (DN)] of the detector and the blackbody radiance can be expressed as [15,16]

$$h = G \cdot L_B(T_b) + B, \tag{1}$$

where h denotes the output gray values of the detector, G denotes the response to the incident blackbody radiance, and B denotes the offset of radiometric calibration including the output caused by the stray radiation in each band and the internal factors of the detector. Both G and B can be obtained by fitting the blackbody radiance at different temperatures to the corresponding outputs. $L_B(T_b)$ is the incident radiance of the reference source at temperature T_b, and it can be calculated by [17,18]

$$L_B(T_b) = \frac{1}{\pi} \cdot \int_{\Delta\lambda_N} \tau_{\text{opt}}(\lambda) \cdot \tau_{\text{fil}}(\lambda) \cdot R_{\text{det}}(\lambda) \cdot L_b(\lambda, T_b) \mathrm{d}\lambda. \tag{2}$$

Here, $\tau_{\text{fil}}(\lambda)$ is the spectral transmittance of the optical filter, and $\Delta\lambda_N$ is the spectral range. $\tau_{\text{opt}}(\lambda)$ is the spectral transmittance of the optical lens, $R_{\text{det}}(\lambda)$ is the spectral response of the detector, and $L_b(\lambda, T_b)$ is the spectral radiance of an ideal blackbody at temperature T_b.

2. Ratio Formula of Dual-Band Thermometry

When viewing a gray-body closely, the influence of atmosphere can be neglected [19]. The total radiation received by the detector consists of the radiation emitted from the target, the reflected ambient radiation, and the stray radiation originating from the optical system and the optical filter, as shown in Fig. 1.

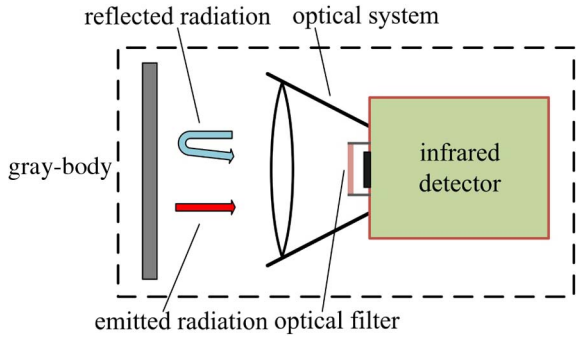

Fig. 1. Measurement model of a dual-band thermometer. The optical system consists of the optical lens, the housing cone, and other mechanical structures.

The output of the detector is given by [20,21]

$$h = G\varepsilon L_B(T_t) + G(1-\varepsilon)L_B(T_{\text{atm}}) + B, \tag{3}$$

where ε is the emissivity of the gray-body, the first two parts of the right side are the contributions of the emitted radiation and the reflected ambient radiation, respectively, and the stray radiation is included in B. $L_B(T_t)$ and $L_B(T_{\text{atm}})$ is the radiance of a blackbody at temperature T_b and T_{amb}, respectively. The measurement formulas of the two bands can then be expressed as

$$h_1 = G_1\varepsilon_1 L_{B1}(T_t) + G_1(1-\varepsilon_1)L_{B1}(T_{\text{atm}}) + B_1, \tag{4}$$

$$h_2 = G_2\varepsilon_2 L_{B2}(T_t) + G_2(1-\varepsilon_2)L_{B2}(T_{\text{atm}}) + B_2. \tag{5}$$

Here, the parameters in Eqs. (4) and (5) have the same implications as mentioned before, where subscripts 1 and 2 are the sequence numbers of the optical filters. Emissivity in different spectral bands can be derived from Eqs. (4) and (5). Under the assumption of equal target emissivity in different bands, the ratio formula for temperature measurement can be expressed as

$$\frac{G_2L_{B2}(T_t) - G_2L_{B2}(T_{\text{atm}})}{G_1L_{B1}(T_t) - G_1L_{B1}(T_{\text{atm}})} = \frac{h_2 - B_2 - G_2L_{B2}(T_{\text{atm}})}{h_1 - B_1 - G_1L_{B1}(T_{\text{atm}})}. \tag{6}$$

Here, the left side of Eq. (6), defined as the calibration radiance ratio of a reference blackbody, is used for calibration. It can be calculated directly using the results of radiometric calibrations. The right side can be used to calculate the measurement radiance ratio of the examined target. The temperature of the target can then be determined by comparing the measurement radiance ratio with the calibration radiance ratio.

B. Ambient Temperature-Independent DMRT

When ambient temperature fluctuates, the offset of radiometric calibration, i.e., parameter B in Eq. (1), will drift, which leads to the radiometric calibration error in each band; furthermore, it results in temperature measurement error. In order to remove this effect, the relation between the calibration offset and the ambient temperature is analyzed.

1. Radiometric Calibration Considering Ambient Temperature

As shown in Eq. (1), the response and offset are the major parameters in the calibration process. For a cooled MWIR detector working at a stabilized temperature, the response of the detector does not vary with the ambient temperature. Therefore, the effect of ambient temperature mainly manifests itself in the offset, i.e., B varies with the ambient temperature.

As analyzed in Section 2.A, the offset originates from the stray radiation and the internal factors of the detector. Only the stray radiation depends on the ambient temperature. The offset can thus be expressed as [22]

$$B(T_{\text{amb}}) = G' \cdot [\Phi_{\text{sys}}(T_{\text{amb}}) + \Phi_{\text{fil}}(T_{\text{amb}})] + h_{\text{detector}}, \quad (7)$$

where G' denotes the response to the radiation flux, and h_{detector} denotes the output caused by internal factors, e.g., the dark current and the cold stop, which would not vary with the ambient temperature for a cooled detector and can be obtained by calibration. The two parts within the square brackets are the two components of stray radiation of the thermometer at ambient temperature T_{amb}, which is a major, non-negligible factor affecting temperature measurements for radiation thermometry [23]. It mainly contains the radiation emitted and reflected from components of the thermometer, e.g., the optical lens, the optical filter, the housing cone, other mechanical structures, and the narcissus signature of the detector [7]. The narcissus signature which is independent of the ambient temperature can be subsumed into h_{detector} for simplification.

The $\phi_{\text{sys}}(T_{\text{amb}})$ is the stray radiation of the optical system which is transmitted by the filter, and it is proportional to the blackbody radiance in the passband of the optical filter at the ambient temperature, as shown in Eq. (8)

$$\Phi_{\text{sys}}(T_{\text{amb}}) = k_1 \cdot L_B(T_{\text{amb}}), \quad (8)$$

where k_1 is the geometrical factor between the radiance and the radiation flux. $\phi_{\text{sys}}(T_{\text{amb}})$ can be considered as the sum of radiation emitted and reflected by many small elements [7]. Thus, k_1 is related to the radiation transmission path, e.g., the transmittance, the area, and the corresponding projected solid angle of each small element.

$\phi_{\text{fil}}(T_{\text{amb}})$ is the stray radiation generated by the filter. It consists of the radiation emitted and reflected by the optical filter, and it strikes the detector directly. According to Kirchhoff's law, the spectral emissivity and spectral absorptivity of a certain material are equal [24]. This means that $\phi_{\text{fil}}(T_{\text{amb}})$ can be regarded as the difference between the ambient radiation in the response waveband of the detector and the ambient radiation transmitting through the optical filter. It can be expressed as

$$\Phi_{\text{fil}}(T_{\text{amb}}) = k_2 \cdot (L_{\text{BA}}(T_{\text{amb}}) - L_B(T_{\text{amb}})), \quad (9)$$

where k_2 is a geometrical factor, and $L_{\text{BA}}(T_{\text{amb}})$ denotes the radiance of an ideal blackbody at temperature T_{amb} in the response waveband of the detector.

Then the offset $B(T_{\text{amb}})$ can be written as

$$B(T_{\text{amb}}) = m_1 \cdot L_{\text{BA}}(T_{\text{amb}}) + m_2 \cdot L_B(T_{\text{amb}}) + h_{\text{detector}}. \quad (10)$$

Here, $m_1 = G' \times k_2$, and $m_2 = G' \times (k_1 - k_2)$. As shown in Eq. (10), the offset under a certain ambient temperature is a linear combination of the radiance in different spectral bands. In theory, m_1 and m_2 are constants in each band for a given dual-band thermometer, and they can be obtained by fitting the offsets at two different ambient temperatures.

2. Ratio Formula of Dual-Band Thermometry Considering Ambient Temperature

According to Eq. (10), the offset varies with the ambient temperature. This will introduce an error of measurement radiance ratio in Eq. (6); furthermore, it results in a measurement error. Here, we assume that the ambient temperature of initial calibration is T_{amb0} and that it increases to T_{amb} in the subsequent temperature measurement. The offset drift ΔB can then be obtained as

$$\begin{aligned}\Delta B &= B(T_{\text{amb}}) - B(T_{\text{amb0}}) \\ &= m_1[L_{\text{BA}}(T_{\text{amb}}) - L_{\text{BA}}(T_{\text{amb0}})] \\ &\quad + m_2[L_B(T_{\text{amb}}) - L_B(T_{\text{amb0}})]. \end{aligned} \quad (11)$$

To improve the measurement accuracy, the ratio formula considering ambient temperature fluctuation can be written as

$$\frac{G_2 L_{B2}(T_t) - G_2 L_{B2}(T_{\text{atm}})}{G_1 L_{B1}(T_t) - G_1 L_{B1}(T_{\text{atm}})} = \frac{h_2 - (B_2 + \Delta B_2) - G_2 L_{B2}(T_{\text{atm}})}{h_1 - (B_1 + \Delta B_1) - G_1 L_{B1}(T_{\text{atm}})}, \quad (12)$$

where ΔB_1 and ΔB_2 are the offset drifts in different bands. Equation (12) provides a method to remove the effect of ambient temperature fluctuations on dual-band thermometry. In this method, the calibration of a dual-band thermometer does not need to be performed frequently when ambient temperature changes. As a consequence, this method can solve several inevitable problems in practical applications, such as the hostile fields and the time lag between calibration and temperature measurement.

3. EXPERIMENTS AND RESULTS

A. Experiment Setup

To illustrate the conclusions above experimentally, the experiments are performed in three steps. First, we perform radiometric calibration to obtain the parameters of G and B under a certain ambient temperature T_1, and we measure a gray-body to verify the validation of the DMRT considering reflected ambient radiation and stray radiation. Second, we repeat the calibration processes under ambient temperature T_2, combined with the calibration results of T_1. The parameters m_1 and m_2 can be obtained by fitting the offsets of the calibration curves. Finally, the ambient temperature is changed to T_3, and we achieve the temperature measurement results using Eqs. (11) and (12). They are then compared with the results achieved by actual calibration to verify the validation of the ambient temperature-independent DMRT.

The experimental dual-band MWIR thermometer is shown as Fig. 2(a). It consists of a cooled mid-infrared detector, an optical system, and two infrared bandpass interference filters. During the radiometric calibration, we adopted the near-extended-source method, i.e., an accurate, extended blackbody is positioned closely to the optical system so that the

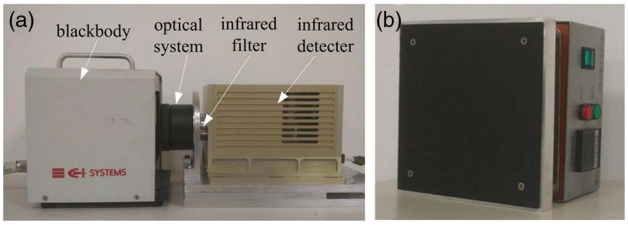

Fig. 2. Experiment setup. (a) The calibration setup. The infrared detector operates in 3.7–4.8 μm waveband, with a 14 bit digital output. The blackbody operates in the temperature range of 0°C to 125°C, and it exhibits an effective emissivity of about 0.97 in the waveband above. The center wavelengths of the two filters are 4520 nm and 4665 nm, respectively. (b) The gray-body. It consists of a constant emissivity plate, a constant temperature heating platform, and a K-type thermocouple. The constant emissivity plate is manufactured by spraying specific paint on an aluminum plate to ensure a constant emissivity (almost 0.86 in the 3.7–4.8 μm wavebands). The aluminum plate is fixed on the surface of a constant temperature heating platform that is used to control the plate's temperature. The K-type thermocouple is spot welded onto the rear side of the gray-body to obtain the real target temperature. The gray-body operates in the range of 30°C to 130°C with an accuracy of 0.2°C.

atmospheric effects can be ignored [25]. The radiation of the blackbody, which is focused by the optical system, transmits through the optical filter and strikes the detector. The two filters are alternately fixed in the optical path to collect incident radiation at different spectral bands. The temperature measurement was performed by replacing the blackbody with a gray-body, as shown in Fig. 2(b). The spectral transmittance of the filters, the spectral response of the detector, and the spectral response of the dual-band thermometer with monochromatic filters is shown in Fig. 3 [26,27].

B. Results and Analysis

To ensure good performance of our method, experiments were conducted in a chamber with a controllable and stable temperature ranging from 0°C to 50°C.

1. Results Considering Reflected Ambient Radiation and Stray Radiation

The ambient temperature of the initial calibration T_{amb0} was set to 8.3°C. To obtain G and B, we calibrated the two bands of the thermometer under T_{amb0}. Then the gray-body was measured at temperatures ranging from 50°C to 120°C, with 10°C intervals. The integration time in our experiment is selected as 1 ms, and different integration times can be selected to accommodate the temperature range of the examined gray-body from 40°C to 230°C.

By using the left side ratio of Eq. (6), the calibration curve A considering the reflected ambient radiation is obtained, and as a comparison, the calibration curve B without this consideration is also illustrated in Fig. 4(a). Obviously, there is a significant difference between them, and the measurement ratios considering reflected ambient radiation and stray radiation are consistent with the calibration curve A. In addition, the curves A and B become closer to each other as the measurement temperature increases. This implies that the effect of the reflected ambient radiation will decrease for a high-temperature target,

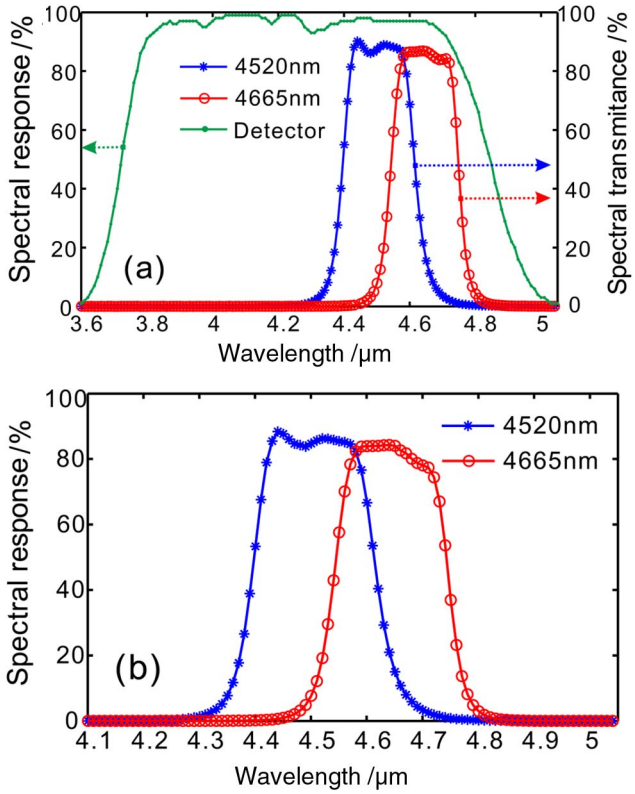

Fig. 3. (a) Spectral transmittance for the 4520 and 4665 nm filters and the spectral response of the detector. (b) Spectral response of the dual-band thermometer with monochromatic filters.

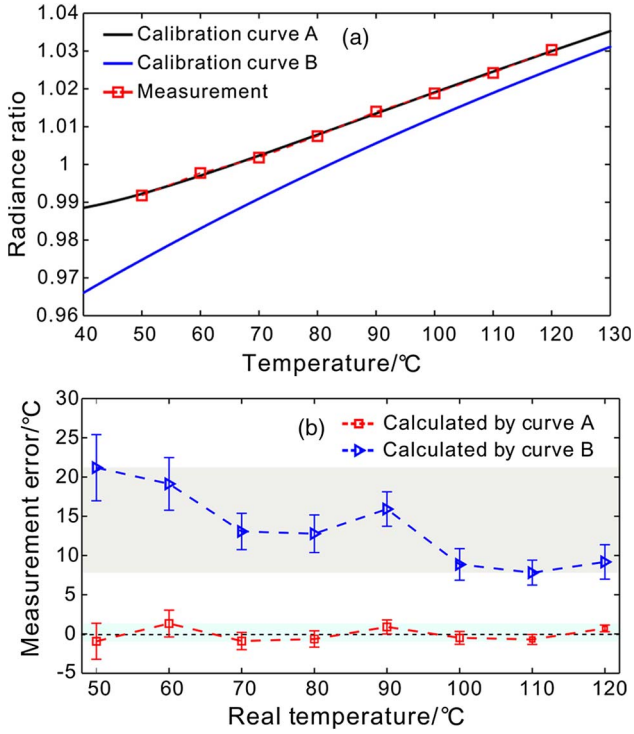

Fig. 4. (a) Ratios of calibration and measurement. (b) Errors of temperature measurement. The error bars represent minimum and maximum values from measurements for ten times.

and it is essential to consider this effect for a low-temperature target in dual-band temperature measurements.

After the calibration, temperature of the gray-body can be obtained by comparing the measurement ratios with the calibration curve. The measurement results are presented in Fig. 4(b). When the reflected ambient radiation and stray radiation are taken into account, the average errors of temperature measurements are not greater than 2°C for the temperature range of 50°C to 120°C. The error curve for temperature measurements using calibration curve A seems to be evenly distributed around zero. The measurement errors are mainly caused by the inaccurate measurement results of the ambient temperature in Eq. (6). In addition, the fluctuating range for each measurement point is less than 4°C and decreases as the target temperature increases, which demonstrates that the accuracy of our method is stable. Without these considerations, the maximum measurement error even reaches 25°C shown as the blue triangles in Fig. 4(b). Therefore, both the reflected ambient radiation and stray radiation should be considered when measuring a low-temperature target.

2. Results under Different Ambient Temperatures

To illustrate the method proposed experimentally, the calibrations were first performed under different ambient temperatures, i.e., 18.5°C, 29.4°C, 37.3°C, and 47.6°C. By use of the calibration results at any two ambient temperatures, m_1 and m_2 in Eq. (10) were obtained by fitting the calibration offsets. Therefore, the corrected offset drifts were calculated by Eq. (11).

The actual offset drift for each band is defined as the difference between offsets at a certain ambient temperature and T_{amb0}, i.e., 8.3°C. As shown in Fig. 5, it increases rapidly with ambient temperature, and the maximum value is nearly 2500 DN (about 15% of the dynamic range of a 14 bit detector). The calculated offset drifts agree well with the actual drifts. Therefore, this method can be used to compensate the effect of ambient temperature fluctuations on the calibration in each band.

Temperature measurements were then conducted under the aforementioned ambient temperatures. The experimental results under 29.4°C are presented in Fig. 6. The corrected measurement ratios (blue triangles) considering the offset drifts were calculated using Eq. (12). The uncorrected ones (green circles) were derived without this consideration, and the actual ones (red rectangles) were calculated by Eq. (6) using the actual offsets in different bands under a certain ambient temperature. The corrected ratios and the actual ratios are coincident with the calibration curve, whereas, the uncorrected ratios seriously deviate from the calibration curve. In addition, as shown in Fig. 7, the corrected measurement errors are in good agreement with that of the actual measurement. The difference between them is caused by the error of the offset estimation. They are less than the uncorrected errors, which proves that our method can remove the effect of ambient temperature fluctuations on dual-band temperature measurements. Besides, as shown in the inset of Fig. 7, the precision of our method under other ambient temperatures is similar to that of 29.4°C, which verifies that our method is valid for dual-band temperature measurements under various ambient temperatures.

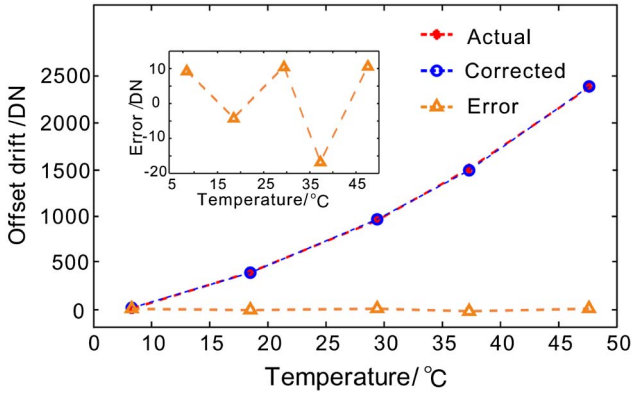

Fig. 5. Calculated offset drifts compared with the real ones. The inset is a close-up of the error.

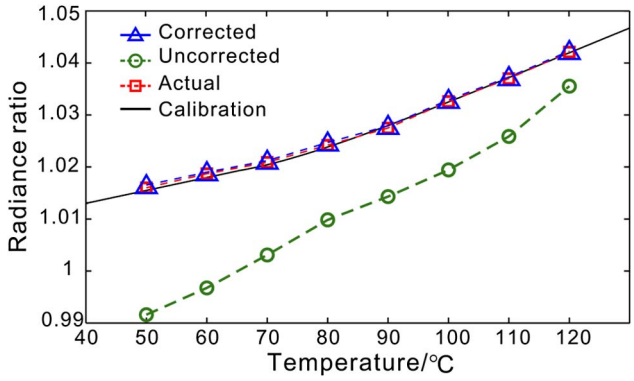

Fig. 6. Ratios compared with the calibration curve.

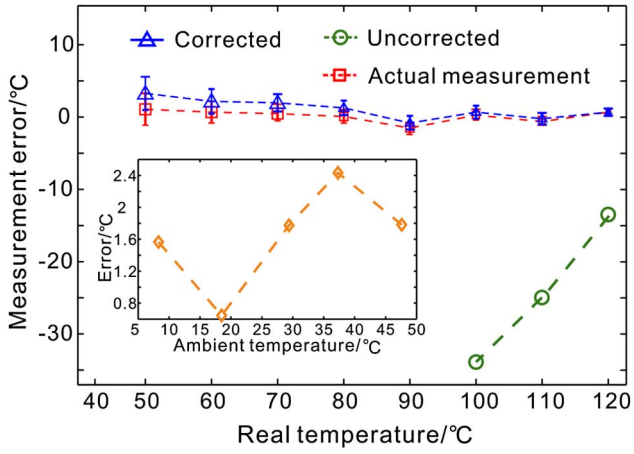

Fig. 7. Measurement errors under 29.4°C. When the target temperature is less than 100°C, the uncorrected errors are larger than 40°C, and they are omitted in the graph. The inset shows the measurement errors of all the temperature points under other ambient temperatures.

4. CONCLUSIONS

This paper proposes dual-band mid-infrared radiation thermometry to measure the low-temperature target by considering

reflected ambient radiation from the examined target and stray radiation inside the measurement system. By analyzing the effect of ambient temperature on calibrations in each band of a dual-band thermometer, an improved method to remove the effect of ambient temperature is deduced. We illustrate theoretically and experimentally that this method can yield high measurement accuracy, and it can remove the effect of ambient temperature fluctuations on dual-band temperature measurements effectively. This method can be used for measuring low-temperature targets, and it also provides an approach to calibrate the dual-band measurement system in the laboratory instead of hostile environments, which can be practical in the application of temperature measurements under various ambient temperatures.

Funding. National Natural Science Foundation of China (NSFC) (61102023).

Acknowledgment. The authors appreciate useful discussions with Yue Wang and Jia-Bin Wu in CIOMP.

REFERENCES

1. C. H. Ma, W. Zhang, and F. W. Meng, "Application of data fusion algorithm at CCD colorimetric temperature measurement," in *IEEE Fifth International Conference on Advanced Computational Intelligence* (IEEE, 2012), pp. 284–286.
2. V. C. Raj and S. V. Prabhu, "Measurement of surface temperature and emissivity of different materials by two-colour pyrometry," Rev. Sci. Instrum. **84**, 124903 (2013).
3. F. Cignoli, S. De Iuliis, V. Manta, and G. Zizak, "Two-dimensional two-wavelength emission technique for soot diagnostics," Appl. Opt. **40**, 5370–5378 (2001).
4. X. Y. Zhang, Q. Cheng, C. Lou, and H. C. Zhou, "An improved colorimetric method for visualization of 2-D, inhomogeneous temperature distribution in a gas fired industrial furnace by radiation image processing," Proc. Combust. Inst. **33**, 2755–2762 (2011).
5. C. Lou, W. H. Li, H. C. Zhou, and C. T. Salinas, "Experimental investigation on simultaneous measurement of temperature distributions and radiative properties in an oil-fired tunnel furnace by radiation analysis," Int. J. Heat Mass Transfer **54**, 1–8 (2011).
6. Y. Ren, X. M. Zhou, and F. Li, "Survey of dual waveband colorimetric temperature measurement technology," Chin. Control Decis. Conf. **26**, 5177–5181 (2014).
7. S. T. Chang, Y. Y. Zhang, Z. Y. Sun, and M. Li, "Method to remove the effect of ambient temperature on radiometric calibration," Appl. Opt. **53**, 6274–6279 (2014).
8. W. Small, P. M. Celliers, L. B. Da Silva, D. L. Matthews, and B. A. Soltz, "Two-color mid-infrared thermometer with a hollow glass optical fiber," Appl. Opt. **37**, 6677–6683 (1998).
9. S. Sade, I. Uman, V. Gopal, J. A. Harrington, and A. Katzir, "Fiberoptic infrared multi-spectral radiometers for emissivity and temperature measurements of gray bodies near room temperatures," Proc. SPIE **5363**, 116–124 (2004).
10. J. Bundas, R. Dinnis, K. Patnaude, D. Burrows, R. Faska, M. Sundaram, A. Reisinger, and D. Manitakos, "Absolute temperature measurements using a two-color QWIP focal plane array," Proc. SPIE **7660**, 76603R (2010).
11. A. Araújo, S. Silvano, and N. Martins, "Monte Carlo uncertainty simulation of surface emissivity at ambient temperature obtained by dual spectral infrared radiometry," Infrared Phys. Technol. **67**, 131–137 (2014).
12. A. Araújo, S. Silvano, and N. Martins, "Monte Carlo simulations of ambient temperature uncertainty determined by dual-band pyrometry," Meas. Sci. Technol. **26**, 085016 (2015).
13. J. R. Dupuis, D. Mansur, R. Vaillancourt, D. Carlson, E. Schundler, and G. Genetti, "Two-band infrared thermographer for standoff temperature measurements," Proc. SPIE **6219**, 62190E (2006).
14. A. Hijazi, S. Sachidanandan, R. Singh, and V. Madhavan, "A calibrated dual-wavelength infrared thermometry approach with non-greybody compensation for machining temperature measurements," Meas. Sci. Technol. **22**, 025106 (2011).
15. H. Lee, C. Oh, and J. W. Hahn, "Calibration of a mid-IR optical emission spectrometer with a 256-array PbSe detector and an absolute spectral analysis of IR signatures," Infrared Phys. Technol. **57**, 50–55 (2013).
16. Z. Y. Sun, S. T. Chang, and W. Zhu, "Radiometric calibration method for large aperture infrared system with broad dynamic range," Appl. Opt. **54**, 4659–4666 (2015).
17. Y. Té, P. Jeseck, I. Pépin, and C. Camy-Peyret, "A method to retrieve blackbody temperature errors in the two points radiometric calibration," Infrared Phys. Technol. **52**, 187–192 (2009).
18. U. Anselmi-Tamburini, G. Campari, G. Spinolo, and P. Lupotto, "A two-color spatial-scanning pyrometer for the determination of temperature profiles in combustion synthesis reactions," Rev. Sci. Instrum. **66**, 5006 (1995).
19. R. R. Crowin and A. Rodenburgh II, "Temperature error in radiation thermometry caused by emissivity and reflectance measurement error," Appl. Opt. **33**, 1950–1957 (1994).
20. M. Voigt, V. Ramesh, J. Vinay, and D. LeMieux, "The effect of surface reflection and surrounding environment on target temperature estimation using an infrared FPA," Proc. SPIE **6541**, 654103 (2007).
21. J. J. Talghader, A. S. Gawarikar, and R. P. Shea, "Spectral selectivity in infrared thermal detection," Light Sci. Appl. **24**, 1–11 (2012).
22. T. R. Fu, M. H. Duan, J. F. Liu, and T. Li, "Spectral stray light effect on high-temperature measurements using a near-infrared multi-wavelength pyrometer," Infrared Phys. Technol. **67**, 590–595 (2014).
23. S. G. R. Salim, N. P. Fox, W. S. Hartree, E. R. Woolloams, T. Sun, and K. T. V. Grattan, "Stray light correction for diode-array-based spectrometers using a monochromator," Appl. Opt. **50**, 5130–5138 (2011).
24. T. R. Fu, J. F. Liu, and A. Z. Zong, "Radiation temperature measurement method for semitransparent materials using one-channel infrared pyrometer," Appl. Opt. **53**, 6830–6839 (2014).
25. G. C. Holst, *Testing and Evaluation of Infrared Imaging Systems* (JCD, 1933).
26. T. R. Fu, H. Zhao, J. Zeng, M. H. Zhong, and C. L. Shi, "Two-color optical CCD-based pyrometer using a two-peak filter," Rev. Sci. Instrum. **81**, 124903 (2010).
27. T. R. Fu, H. Zhao, J. Zeng, Z. Wang, M. H. Zhong, and C. L. Shi, "Improvements of three-color optical CCD-based pyrometer system," Appl. Opt. **49**, 5997–6005 (2010).